Electronic Journal of Qualitative Theory of Differential Equations
2026, No. **29**, 1–26; https://doi.org/10.14232/ejqtde.2026.1.29 www.math.u-szeged.hu/ejqtde/

A stage structured predator–prey system with time delays and fear effect

Lingrui Li[1], **Junli Liu**[✉1] and **Tailei Zhang**[2]

[1]School of Science, Xi'an Polytechnic University, Xi'an, 710048, P.R. China
[2]School of Science, Chang'an University, Xi'an, 710064, P.R. China

Received 10 October 2025, appeared 21 July 2026
Communicated by Ferenc Hartung

Abstract. In this study, we develop a delayed predator–prey model that incorporates two stage structures for both predator and prey populations, along with two constant maturation delays and fear effect. The model is formulated as a delay differential equation system, and its well-posedness is rigorously demonstrated. We conduct a comprehensive analysis of the system, including stability evaluations and the identification of Hopf bifurcations caused by the delay terms. Numerical simulations are used to validate and extend the theoretical findings, leading to several key insights. Notably, variations in the delay parameters significantly affect the stability of the system. With a single delay, the system undergoes a transition from stability to oscillation and back to stability as the delay increases, showing a characteristic stability-oscillation-stability pattern. Furthermore, when both delays are taken into account, extrema-based bifurcation diagrams and time series reveal multi-branch structures, periodic windows, and complex irregular oscillatory segments. Delay-embedding phase portraits uncover typical patterns such as period-doubling cascades and the reappearance of periodic windows. Additionally, two types of numerical diagnostics provide further evidence: significant sensitivity to initial histories is observed in the complex segment, while coexisting attractors are detected in the branch-splitting segment, suggesting bistability in the system. These results indicate that stage structure coupled with dual maturation delays can significantly enrich the bifurcation structure and long-term dynamical behavior of the system.

Keywords: time delay, stage structure, fear effect, stability, Hopf bifurcation.

2020 Mathematics Subject Classification: 34K13, 34K20, 37N25, 92B05.

1 Introduction

In natural ecosystems, stage structure and time delays are two fundamental ecological mechanisms that shape population's dynamics [1,10]. Most species experience developmental transitions from juvenile to adult stages, with individuals at each stage exhibiting distinct mortality rates, feeding capacities, and other life-history traits. In particular, juveniles are subject to considerable mortality prior to maturation, which can significantly influence the dynamics of the

✉Corresponding author. Email: jlliu2008@126.com

system[4]. In addition to direct predation, the presence of predators often triggers behavioral adaptations in prey, a phenomenon known as the fear effect. This non-consumptive interaction suppresses foraging, reproduction and movement of the prey. As a result, it indirectly reduces prey's growth and alters the predator–prey interaction structure [12, 15, 17, 20, 23, 25, 27]. Although the fear effect has been extensively supported by empirical studies, its incorporation into delay differential equation (DDE) models remains limited.

It has been well established that both time delays [2, 5, 16, 26] and stage structure [18, 28] are capable of inducing complex dynamical behaviors on their own, such as loss of stability, emergence of periodic solutions, Hopf bifurcations, and even chaos [3,29]. For example, Gourley and Kuang [11] analyzed a stage-structured predator–prey model with maturation delay and juvenile mortality, systematically examining their effects on system stability. Their results showed that when juvenile's mortality is non-zero, the system exhibits globally stable equilibria for both short and long delays, but sustained oscillations arise within an intermediate delay range. In contrast, when the mortality of the juvenile is absent, oscillatory behavior persists and intensifies with increasing delay. Recent studies have started incorporating the fear effect into delayed ecological models [6, 22]. Moreover, Ma et al. [21] proposed a predator–prey model incorporating both maturation delay of the prey and the fear effect. Using a combination of theoretical analysis and numerical simulations, they demonstrated that increasing the maturation delay can eliminate both stable and unstable periodic orbits and may stabilize an otherwise unstable positive equilibrium. These findings highlight the complex interplay between maturation delay and fear effects in regulating population dynamics.

Motivated by these insights, this study introduces a delayed predator–prey model that incorporates stage structures for both prey and predators, along with two discrete time delays. The aim is to examine the combined effects of stage structure, maturation delay and the fear effect, and to enhance our understanding of how these factors jointly regulate ecological interactions. The remainder of the paper is organized as follows. In Section 2, we formulate the mathematical model, which includes juvenile and adult stages for both species, along with two discrete delays. We demonstrate that the dynamics of juvenile is entirely determined by the historical states of the adult populations, which enables a reduction of the system to a delay differential equation system involving only adult variables. The well-posedness of the model is rigorously established by proving the existence, uniqueness, non-negativity, and boundedness of its solutions. Section 3 presents some results on the stability of equilibria, existence of Hopf bifurcation. In Section 4, we provide numerical simulations. Section 5 summarizes the key findings and discusses possible extensions and future research directions.

2 Model formulation

In this section, we will develop a delayed predator–prey model that incorporates population stage structure and maturation delays. Both of the predators and prey are divided into two stages: the juvenile and the adult. Our model is described by the following differential equa-

tions with two discrete delays

$$\begin{aligned}
\frac{dx_1(t)}{dt} &= \frac{r_0 x(t)}{1+ky(t)} - \frac{r_0 e^{-d_1\tau_1} x(t-\tau_1)}{1+ky(t-\tau_1)} - d_1 x_1(t),\\
\frac{dx(t)}{dt} &= \frac{r_0 e^{-d_1\tau_1} x(t-\tau_1)}{1+ky(t-\tau_1)} - d_2 x(t) - ax^2(t) - P(x(t))y(t),\\
\frac{dy_1(t)}{dt} &= bP(x(t))y(t) - be^{-m_1\tau_2} P(x(t-\tau_2))y(t-\tau_2) - m_1 y_1(t),\\
\frac{dy(t)}{dt} &= be^{-m_1\tau_2} P(x(t-\tau_2))y(t-\tau_2) - m_2 y(t).
\end{aligned} \tag{2.1}$$

Here, $x_1(t)$, $x(t)$, $y_1(t)$, and $y(t)$ denote the population densities of juvenile prey, adult prey, juvenile predators and adult predators at time t, respectively. The parameter r_0 represents the intrinsic growth rate of the prey, while k describes the fear level of the prey to the predator. The death rates of juvenile and adult prey are denoted by d_1 and d_2, respectively, and a denotes the intraspecific competition coefficient among adult prey. The function $P(x(t))$ describes the functional response of adult predators, while b denotes the energy conversion efficiency of adult predators after consuming adult prey. The death rates of juvenile and adult predators are denoted by m_1 and m_2, respectively. The parameters τ_1 and τ_2 represent the developmental time delays from juvenile to adult stages for prey and predators, respectively. The terms $e^{-d_1\tau_1}$ and $e^{-m_1\tau_2}$ denote the survival probabilities of juvenile prey and juvenile predators during the respective delay periods.

It is straightforward to see that the first and third equations can be equivalently rewritten in the following integral forms

$$\begin{aligned}
x_1(t) &= \int_{t-\tau_1}^{t} \frac{r_0 x(\rho)}{1+ky(\rho)} e^{-d_1(t-\rho)} d\rho,\\
y_1(t) &= \int_{t-\tau_2}^{t} bP(x(\rho))y(\rho) e^{-m_1(t-\rho)} d\rho.
\end{aligned} \tag{2.2}$$

These expressions indicate that $x_1(t)$ and $y_1(t)$ depend entirely on the historical states of $x(t)$ and $y(t)$, and therefore do not contribute additional dynamic complexity. As a result, the long-term behavior of the system is determined by the remaining two equations, prompting the consideration of the reduced model below

$$\begin{aligned}
\frac{dx(t)}{dt} &= \frac{r_0 e^{-d_1\tau_1} x(t-\tau_1)}{1+ky(t-\tau_1)} - d_2 x(t) - ax^2(t) - P(x(t))y(t),\\
\frac{dy(t)}{dt} &= be^{-m_1\tau_2} P(x(t-\tau_2))y(t-\tau_2) - m_2 y(t).
\end{aligned} \tag{2.3}$$

All parameters r_0, d_1, k, d_2, a, b, m_1 and m_2 are assumed to be positive constants, while τ_1 and τ_2 are non-negative constants. In addition, the function $P(x)$ is assumed to be differentiable and satisfy the following properties

$$P(0) = 0, \quad P'(x) > 0 \quad \text{and} \quad \frac{P(x)}{x} \text{ is bounded for all } x \geq 0. \tag{2.4}$$

Typical choices for $P(x)$ satisfying (2.4) include the linear form $P(x) = cx$, the Holling type II form $P(x) = \frac{cx}{1+qx}$, and the Holling type III form $P(x) = \frac{cx^2}{1+qx^2}$, where $c, q > 0$ are constants.

Based on biological considerations, the initial conditions for model (2.3) are given as follows

$$(x(\psi), y(\psi)) = (x_0(\psi), y_0(\psi)) \in \mathcal{C}\left([-\tau, 0], \mathbb{R}^2_+\right) =: \mathcal{C}_+, \qquad \tau = \max\{\tau_1, \tau_2\}, \tag{2.5}$$

where $\mathcal{C}_+$ denotes the Banach space of continuous functions from $[-\tau, 0]$ to $\mathbb{R}^2_+$.

Next, we first prove the well-posedness of model (2.3).

Theorem 2.1. *With initial condition (2.5), model (2.3) admits a unique nonnegative solution for $t \geq 0$. Moreover, the following assertions hold: If $r_0 e^{-d_1\tau_1} \leq d_2$, then $\lim_{t\to\infty} x(t) = 0$, $\lim_{t\to\infty} y(t) = 0$; If $r_0 e^{-d_1\tau_1} > d_2$, then all positive solutions are ultimately bounded. Furthermore, the bounded set*

$$\Omega := \left\{(x(t), y(t)) \in \mathcal{C}_+ : 0 \leq x(t) \leq \frac{r_0 e^{-d_1\tau_1} - d_2}{a},\ 0 \leq x(t-\tau_2) + \frac{1}{b} e^{m_1\tau_2} y(t) \leq L_0\right\}$$

attracts all positive solutions of (2.3), where

$$L_0 := \frac{r_0 e^{-d_1\tau_1}\left(r_0 e^{-d_1\tau_1} - d_2\right)}{\delta a},$$

with $\delta = \min\{d_2, m_2\}$.

Proof. The existence and uniqueness of the solution follows from the method of steps [13]. Let $\hat{\tau} = \min\{\tau_1, \tau_2\}$. Since we assume $x(\psi) \geq 0$ and $y(\psi) \geq 0$ for $-\hat{\tau} \leq \psi \leq 0$, then for $0 \leq t \leq \hat{\tau}$, we have

$$\begin{cases} \dfrac{dx(t)}{dt} \geq -d_2 x(t) - a x^2(t) - P(x(t))\, y(t), \\ \dfrac{dy(t)}{dt} \geq -m_2 y(t). \end{cases}$$

then $x(t) \geq 0$, $y(t) \geq 0$ on this interval by a standard comparison argument. These arguments can be repeated to deduce non-negativity of $x(t)$ and $y(t)$ on $[n\hat{\tau}, (n+1)\hat{\tau}]$, $n = 1, 2, \ldots$, and hence for all $t \geq 0$ indeed. If $r_0 e^{-d_1\tau_1} < d_2$, then Lemma 2 in [19] and a comparison principle gives $\lim_{t\to\infty} x(t) = 0$. If $r_0 e^{-d_1\tau_1} = d_2$, we consider the delay equation $\frac{d\hat{x}(t)}{dt} = d_2\,\hat{x}(t-\tau_1) - d_2\hat{x}(t) - a\hat{x}^2(t)$. Let $V(t) = \hat{x}(t) + d_2 \int_{t-\tau_1}^{t} \hat{x}(s)\, ds$. Then $\frac{dV(t)}{dt} = -a\hat{x}^2(t) \leq 0$, and $\frac{dV(t)}{dt} = 0$ if and only if $\hat{x}(t) = 0$. Consequently, by the comparison principle, we obtain $\lim_{t\to\infty} x(t) = 0$. Therefore, if $r_0 e^{-d_1\tau_1} \leq d_2$, then $\lim_{t\to\infty} x(t) = 0$. Since $P(x)$ is differentiable and $P(0) = 0$, then there exists $\eta > 0$ such that $be^{-m_1\tau_2} P(\eta) < m_2$. And also there exists $T_1 > 0$ such that $x(t) < \eta$ for $t \geq T_1$. Hence, for $t \geq T_1 + \tau_2$, we have $\frac{dy(t)}{dt} = be^{-m_1\tau_2} P(x(t-\tau_2)) y(t-\tau_2) - m_2 y(t) \leq be^{-m_1\tau_2} P(\eta) y(t-\tau_2) - m_2 y(t)$. By comparison principle, $y(t)$ is bounded above by the solution $u(t)$ of

$$\frac{du(t)}{dt} = be^{-m_1\tau_2} P(\eta) u(t-\tau_2) - m_2 u(t), \quad t \geq T_1 + \tau_2,$$

satisfying $u(t) = y(t)$ for $t \in [T_1, T_1 + \tau_2]$. Since $be^{-m_1\tau_2} P(\eta) < m_2$, Lemma 1 in [11] yields that $u(t) \to 0$. Thus, $y(t) \to 0$ as $t \to \infty$.

Note that

$$\begin{aligned} \frac{dx(t)}{dt} &= \frac{r_0 e^{-d_1\tau_1} x(t-\tau_1)}{1 + k y(t-\tau_1)} - d_2 x(t) - a x^2(t) - P(x(t)) y(t) \\ &\leq r_0 e^{-d_1\tau_1} x(t-\tau_1) - d_2 x(t) - a x^2(t). \end{aligned}$$

This inequality implies that $x(t)$ is bounded above by the solution of the comparison equation $W'(t) = r_0 e^{-d_1\tau_1} W(t-\tau_1) - d_2 W(t) - aW^2(t)$. If $r_0 e^{-d_1\tau_1} > d_2$, it follows from Lemma 2 in [19] that for positive initial data, we have $\lim_{t\to\infty} W(t) = \frac{r_0 e^{-d_1\tau_1} - d_2}{a}$. By the comparison principle, we obtain $\limsup_{t\to\infty} x(t) \le \frac{r_0 e^{-d_1\tau_1} - d_2}{a}$. Therefore, $x(t)$ is ultimately bounded. As a result, for any $\varepsilon > 0$, there exists $t_0 > 0$ such that $x(t) \le \frac{r_0 e^{-d_1\tau_1} - d_2}{a} + \varepsilon, t > t_0$. Let $L(t) = x(t-\tau_2) + \frac{1}{b} e^{m_1\tau_2} y(t)$. Then

$$\begin{aligned}
\frac{dL(t)}{dt} &= \frac{r_0 x(t-\tau_1-\tau_2)}{1+ky(t-\tau_1-\tau_2)} e^{-d_1\tau_1} - d_2 x(t-\tau_2) - ax^2(t-\tau_2) - \frac{m_2}{b} e^{m_1\tau_2} y(t) \\
&\le r_0 x(t-\tau_1-\tau_2) e^{-d_1\tau_1} - \delta L(t) \\
&\le r_0 e^{-d_1\tau_1} \left(\frac{r_0 e^{-d_1\tau_1} - d_2}{a} + \varepsilon \right) - \delta L(t), \quad t \ge t_0 + \tau_1 + \tau_2,
\end{aligned}$$

This implies that $\limsup_{t\to\infty} L(t) \le \frac{r_0 e^{-d_1\tau_1}\left(r_0 e^{-d_1\tau_1} - d_2\right)}{\delta a} + \frac{r_0 e^{-d_1\tau_1}}{\delta}\varepsilon$. Since $\varepsilon > 0$ was arbitrary, we conclude that $\limsup_{t\to\infty} L(t) \le \frac{r_0 e^{-d_1\tau_1}\left(r_0 e^{-d_1\tau_1} - d_2\right)}{\delta a} =: L_0$.

Therefore, the solution of model (2.3) exists globally and is ultimately bounded. Hence Ω is globally attractive. □

3 Threshold dynamics

This section is devoted to the analysis of the equilibria and their stability for model (2.3). We begin by investigating the existence of equilibria.

Let $\widetilde{E} = (\widetilde{x}, \widetilde{y})$ be an arbitrary equilibrium of model (2.3). Then $\widetilde{E}$ satisfies the following system

$$\begin{aligned}
\frac{r_0 e^{-d_1\tau_1}\widetilde{x}}{1+k\widetilde{y}} - d_2\widetilde{x} - a\widetilde{x}^2 - P(\widetilde{x})\widetilde{y} = 0, \\
be^{-m_1\tau_2} P(\widetilde{x})\widetilde{y} - m_2\widetilde{y} = 0.
\end{aligned} \tag{3.1}$$

It is easy to see that model (2.3) always admits the trivial equilibrium $E_0 = (0,0)$. In addition, if $r_0 e^{-d_1\tau_1} > d_2$, there exists a predator-free equilibrium $E_1 = (x_1, 0)$, where

$$x_1 = \frac{r_0 e^{-d_1\tau_1} - d_2}{a}. \tag{3.2}$$

Furthermore, a positive equilibrium $E^* = (x^*, y^*)$ exists if equation (3.1) admits a positive root. From the second equation of (3.1), we obtain

$$P(x^*) = \frac{m_2 e^{m_1\tau_2}}{b}, \quad \text{that is,} \quad x^* = P^{-1}\left(\frac{m_2 e^{m_1\tau_2}}{b}\right),$$

and y^* is a positive root of the following quadratic equation

$$Ay^{*2} + By^* + C = 0 \tag{3.3}$$

where

$$A = kP(x^*), \quad B = P(x^*) + k(d_2 x^* + a(x^*)^2), \quad C = d_2 x^* + a(x^*)^2 - r_0 x^* e^{-d_1\tau_1}.$$

It is clear that equation (3.3) admits a unique positive root $y^* = \frac{-B+\sqrt{B^2-4AC}}{2A}$ (contains both τ_1 and τ_2) if and only if the following condition holds

$$d_2 + ax^* - r_0 e^{-d_1\tau_1} < 0. \tag{3.4}$$

We point out that, by the monotonicity of function $P(x)$, (3.4) is equivalent to

$$m_2 < bP(x_1)e^{-m_1\tau_2}. \tag{3.5}$$

The above result indicates that the existence of the predator-free equilibrium E_1 and the positive equilibrium E^* crucially depends on the delay parameters τ_1 and τ_2. We now proceed to analyze the stability of the equilibria $E_0 = (0,0)$, $E_1 = (x_1, 0)$ and $E^* = (x^*, y^*)$, which is essential for understanding the dynamics of model (2.3).

Linearizing system (2.3) around the general equilibrium $\widetilde{E} = (\widetilde{x}, \widetilde{y})$ gives

$$\begin{aligned}\frac{dx(t)}{dt} &= \frac{r_0 e^{-d_1\tau_1}}{1+k\widetilde{y}}x(t-\tau_1) - \frac{kr_0 e^{-d_1\tau_1}\widetilde{x}}{(1+k\widetilde{y})^2}y(t-\tau_1)\\ &\quad - d_2 x(t) - 2a\widetilde{x}x(t) - P(\widetilde{x})y(t) - P'(\widetilde{x})\widetilde{y}x(t),\\ \frac{dy(t)}{dt} &= be^{-m_1\tau_2}\widetilde{y}P'(\widetilde{x})x(t-\tau_2) + be^{-m_1\tau_2}P(\widetilde{x})y(t-\tau_2) - m_2 y(t).\end{aligned} \tag{3.6}$$

The stability result about E_0 is stated as follows.

Theorem 3.1. *The trivial equilibrium $E_0 = (0,0)$ is globally asymptotically stable if $d_2 \geq r_0 e^{-d_1\tau_1}$; otherwise, it is unstable.*

Proof. From equation (3.6), the characteristic equation at $E_0 = (0,0)$ is given by

$$(\lambda + m_2)\left(\lambda + d_2 - r_0 e^{-d_1\tau_1}e^{-\lambda\tau_1}\right) = 0.$$

This equation has a negative root $-m_2$, and the remaining roots are determined by

$$g(\lambda) := \lambda + d_2 - r_0 e^{-d_1\tau_1}e^{-\lambda\tau_1} = 0.$$

According to Theorem 3.2.1 in [14], if $d_2 < r_0 e^{-d_1\tau_1}$, $g(\lambda)$ has a positive root, implying that $E_0 = (0,0)$ is unstable. When $d_2 > r_0 e^{-d_1\tau_1}$, all the roots of $g(\lambda) = 0$ have negative real parts, and thus $E_0 = (0,0)$ is locally asymptotically stable. Moreover, based on the proof of Theorem 2.1, if $d_2 \geq r_0 e^{-d_1\tau_1}$, then $x(t) \to 0$ and $y(t) \to 0$ as $t \to \infty$. Therefore, E_0 is globally asymptotically stable. □

Theorem 3.2. *The predator-free equilibrium $E_1 = (x_1, 0)$ exists if and only if $d_2 < r_0 e^{-d_1\tau_1}$. If (3.5) is reversed, then E_1 is globally asymptotically stable in the interior of Ω. If (3.5) is satisfied, then E_1 is unstable.*

Proof. The characteristic equation at E_1 takes the form

$$f_1(\lambda)f_2(\lambda) = 0, \tag{3.7}$$

where

$$\begin{aligned}f_1(\lambda) &= \lambda - r_0 e^{-d_1\tau_1}e^{-\lambda\tau_1} + r_0 e^{-d_1\tau_1} + ax_1,\\ f_2(\lambda) &= \lambda - bP(x_1)e^{-m_1\tau_2}e^{-\lambda\tau_2} + m_2.\end{aligned}$$

Again, by Theorem 3.2.1 in [14], all roots of $f_1(\lambda) = 0$ have negative real parts. When $m_2 > bP(x_1)e^{-m_1\tau_2}$(i.e., (3.5) is reversed), all roots of $f_2(\lambda) = 0$ have negative real parts, and hence E_1 is locally asymptotically stable. Conversely, if $m_2 < bP(x_1)e^{-m_1\tau_2}$, then $f_2(\lambda) = 0$ has at least one root with positive real part, and E_1 is unstable. We consider the case when $m_2 > bP(x_1)e^{-m_1\tau_2}$, then there exists a sufficiently small $\varepsilon > 0$ such that $m_2 > bP(x_1+\varepsilon)e^{-m_1\tau_2}$.

As shown in Section 2,

$$\limsup_{t\to\infty} x(t) \leq \frac{r_0 e^{-d_1\tau_1} - d_2}{a}. \tag{3.8}$$

This implies the existence of $T_\varepsilon > 0$ such that $x(t) < x_1 + \varepsilon$ for all $t \geq T_\varepsilon$. For all $t \geq T_\varepsilon + \tau_2$,

$$\frac{dy(t)}{dt} \leq be^{-m_1\tau_2} P\left(x_1+\varepsilon\right) y\left(t-\tau_2\right) - m_2 y(t).$$

Since $m_2 > bP(x_1+\varepsilon)e^{-m_1\tau_2}$, by Lemma 1 in [11] and the comparison principle, it follows that $y(t) \to 0$ as $t \to \infty$. Hence, for any $\xi \in (0,1)$, there exists $T_\xi > 0$ such that for all $t \geq T_\xi$, $y(t) < \xi$. Since $P(x)/x$ is bounded, there exists a constant $G > 0$ such that

$$\frac{P(x)}{x} \leq G, \quad \text{for all } x > 0.$$

Moreover, since $r_0 e^{-d_1\tau_1} > d_2$, we can choose $\xi > 0$ such that

$$\frac{r_0 e^{-d_1\tau_1}}{1+k\xi} > d_2 + G\xi.$$

We then have

$$P\left(x(t)\right) y(t) = \frac{P(x(t))}{x(t)} x(t) y(t) \leq G\xi x(t).$$

Therefore, for all $t \geq T_\xi + \tau_1$,

$$x'(t) \geq \frac{r_0 e^{-d_1\tau_1}}{1+k\xi} x\left(t-\tau_1\right) - \left(d_2 + G\xi\right) x(t) - ax^2(t).$$

Applying Lemma 2 in [19], together with a comparison argument,

$$\liminf_{t\to\infty} x(t) \geq \frac{\frac{r_0 e^{-d_1\tau_1}}{1+k\xi} - (d_2+G\xi)}{a}.$$

Since ξ was arbitrary, it follows that $\liminf_{t\to\infty} x(t) \geq x_1$, which together with (3.8) implies

$$\lim_{t\to\infty} x(t) = x_1.$$

Hence, the predator-free equilibrium $E_1 = (x_1, 0)$ is globally asymptotically stable in the interior of Ω. □

Remark 3.3. The existence and stability of equilibria in model (2.3) depend critically on system parameters and time delays. If $d_2 \geq r_0 e^{-d_1\tau_1}$, then the model admits only the trivial equilibrium $E_0 = (0,0)$, which is globally asymptotically stable. Conversely, if $d_2 < r_0 e^{-d_1\tau_1}$, then E_0 becomes unstable, and a predator-free equilibrium $E_1 = (x_1, 0)$ emerges, where $x_1 = \frac{r_0 e^{-d_1\tau_1} - d_2}{a}$. Furthermore, if $m_2 > bP(x_1)e^{-m_1\tau_2}$, then E_1 is globally asymptotically stable. In contrast, if $m_2 < bP(x_1)e^{-m_1\tau_2}$, then E_1 becomes unstable and a positive equilibrium $E^* = (x^*, y^*)$ exists. This analysis reveals various stability transitions induced by time delays and parameter variations, highlighting the complex dynamic behavior of the model.

We now turn our attention to the stability of the positive equilibrium $E^* = (x^*, y^*)$, which is crucial for understanding the long-term dynamics of the predator–prey system. To this end, we assume $P(x) = cx$ and that condition (3.4) holds, ensuring the feasibility of E^*. At $E^* = (x^*, y^*)$, the corresponding characteristic equation is given by

$$\begin{vmatrix} \lambda - (d_2 + ax^* + cy^*)\, e^{-\lambda\tau_1} + (d_2 + 2ax^* + cy^*) & \dfrac{kr_0x^*e^{-d_1\tau_1}e^{-\lambda\tau_1}}{(1+ky^*)^2} + cx^* \\ -bcx^*y^*e^{-m_1\tau_2}e^{-\lambda\tau_2} & \lambda + m_2 - m_2e^{-\lambda\tau_2} \end{vmatrix} = 0. \tag{3.9}$$

It is straightforward to verify that $\lambda = 0$ is not a root of equation (3.9). We are interested in whether stability switches occur as the time delays increase. Therefore, we analyze equation (3.9) under four different scenarios.

Case 1: $\tau_1 = 0$, $\tau_2 = 0$. This corresponds to the absence of stage-structure in both prey and predator populations. In this case, the characteristic equation simplifies to the following quadratic form

$$\lambda^2 + ax^*\lambda + \left(\frac{kr_0}{(1+ky^*)^2} + c\right) bcx^*y^* = 0. \tag{3.10}$$

Both the coefficient of λ and the constant term in (3.10) are positive, implying that all roots of (3.10) have negative real parts. Therefore, when both delays are zero, the positive equilibrium is locally asymptotically stable.

In this case, the model reduces to the following ODE system

$$\begin{aligned} \frac{dx(t)}{dt} &= \frac{r_0}{1+ky(t)}x(t) - d_2x(t) - ax^2(t) - cx(t)y(t), \\ \frac{dy(t)}{dt} &= bcx(t)y(t) - m_2y(t). \end{aligned}$$

According to Theorem 3.2 in [27], this positive equilibrium is globally asymptotically stable.

Case 2: $\tau_1 = 0$, $\tau_2 > 0$. In this case, only the stage structure of predators is considered. The corresponding characteristic equation at E^* is given by

$$\lambda^2 + K_1(\tau_2)\lambda + K_2(\tau_2) + (K_3\lambda + K_4(\tau_2))\, e^{-\lambda\tau_2} = 0. \tag{3.11}$$

where

$$\begin{aligned} &K_1(\tau_2) = m_2 + ax^*, \quad K_2(\tau_2) = am_2x^*, \quad K_3 = -m_2, \\ &K_4(\tau_2) = -m_2ax^* + bcy^*\left(\frac{kr_0x^*}{(1+ky^*)^2} + cx^*\right)e^{-m_1\tau_2}. \end{aligned}$$

Assuming $\tau_2 > 0$, we let $\lambda = i\omega$ (with $\omega > 0$) be a root of equation (3.11). Substituting this into (3.11) and separating real and imaginary parts, we obtain

$$\begin{aligned} \omega^2 - K_2(\tau_2) &= K_3\omega\sin\omega\tau_2 + K_4(\tau_2)\cos\omega\tau_2, \\ K_1(\tau_2)\omega &= K_4(\tau_2)\sin\omega\tau_2 - K_3\omega\cos\omega\tau_2. \end{aligned} \tag{3.12}$$

Then ω must be a solution of

$$F(\omega, \tau_2) := \omega^4 + C_1(\tau_2)\omega^2 + C_2(\tau_2) = 0, \tag{3.13}$$

where

$$\begin{aligned} C_1(\tau_2) &= K_1^2(\tau_2) - 2K_2(\tau_2) - K_3^2 = (ax^*)^2 > 0, \\ C_2(\tau_2) &= K_2^2(\tau_2) - K_4^2(\tau_2). \end{aligned}$$

Under the assumption that $\tau_1 = 0$, we have $x^* = \frac{m_2 e^{m_1\tau_2}}{bc}$, y^* is the unique positive root of Eq. (3.3), and in this case it depends only on τ_2. Moreover, inequality (3.4) becomes

$$\tau_2 < \frac{1}{m_1}\ln\left(\frac{bc(r_0-d_2)}{m_2 a}\right) =: \tau_2^*. \tag{3.14}$$

Note that

$$K_2(\tau_2) + K_4(\tau_2) = bcy^*\left(\frac{kr_0x^*}{(1+ky^*)^2} + cx^*\right)e^{-m_1\tau_2} > 0.$$

If $K_2(\tau_2) - K_4(\tau_2) \geq 0$, then equation (3.13) has no positive root, and the positive equilibrium $E^* = (x^*, y^*)$ is locally asymptotically stable for all $\tau_2 \in [0, \tau_2^*)$. If $K_2(\tau_2) - K_4(\tau_2) < 0$, then equation (3.13) admits a unique positive root

$$\omega_1 = \sqrt{\frac{-C_1(\tau_2) + \sqrt{\Delta_1}}{2}}, \quad \text{where } \Delta_1 = C_1^2(\tau_2) - 4C_2(\tau_2).$$

From equation (3.12), we obtain

$$\begin{aligned}
\sin w\tau_2 &= \frac{K_3(\tau_2)w(w^2 - K_2(\tau_2)) + K_1(\tau_2)K_4(\tau_2)w}{K_4^2(\tau_2) + K_3^2(\tau_2)w^2} =: Q_1(\tau_2),\\
\cos w\tau_2 &= \frac{K_4^2(\tau_2)(w^2 - K_2(\tau_2)) - K_1(\tau_2)K_3(\tau_2)w^2}{K_4^2(\tau_2) + K_3^2(\tau_2)w^2} =: P_1(\tau_2).
\end{aligned} \tag{3.15}$$

$I_1 = \{\tau_2 : \tau_2 \in [0, \tau_2^*),\ k_2(\tau_2) < k_4(\tau_2)\}$. Define the function $\theta(\tau_2) \in [0, 2\pi]$, such that $\sin\theta(\tau_2)$ and $\cos\theta(\tau_2)$ are equal to the right-hand sides of the first and second equations in (3.15), respectively. That is,

$$\sin\theta(\tau_2) = Q_1(\tau_2), \qquad \cos\theta(\tau_2) = P_1(\tau_2).$$

Then we have

$$\omega_1(\tau_2)\tau_2 = \theta(\tau_2) + 2n\pi, \quad n = 0, 1, 2, \ldots,$$

which is equivalent to

$$S_n(\tau_2) := \tau_2 - \frac{\theta(\tau_2) + 2n\pi}{\omega_1(\tau_2)} = 0, \quad n = 0, 1, 2, \ldots. \tag{3.16}$$

Actually from equation (3.15), it follows that the expression for $\theta(\tau_2)$ is given by

$$\theta(\tau_2) = \begin{cases} \arccos P_1(\tau_2) & \text{if } Q_1(\tau_2) > 0,\\ 2\pi - \arccos P_1(\tau_2) & \text{if } Q_1(\tau_2) < 0. \end{cases}$$

Then the value of τ_2 at which a stability switch occurs is given by the solution of equation (3.16). To confirm the occurrence of a Hopf bifurcation, the transversality condition must be verified. If there exists $\hat{\tau}_2 \in I_1$ such that $S_n(\hat{\tau}_2) = 0$, then $\pm i\omega_1(\hat{\tau}_2)$ are a pair of simple pure imaginary roots of equation (3.11), and the following result holds.

According to Theorem 4.1 in [4], we have

Theorem 3.4. *Denote*

$$\delta_1(\hat{\tau}_2) := \operatorname{sign}\left\{\frac{d\,\mathrm{Re}\,\lambda}{d\tau_2}\bigg|_{\lambda=i\omega_1(\hat{\tau}_2)}\right\} = \operatorname{sign}\left\{\frac{dS_n(\tau_2)}{d\tau_2}\bigg|_{\tau_2=\hat{\tau}_2}\right\}.$$

The pair $\pm i\,\omega_1(\hat{\tau}_2)$ crosses the imaginary axis from left to right if $\delta_1(\hat{\tau}_2) = 1$, and from right to left if $\delta_1(\hat{\tau}_2) = -1$.

Case 3: $\tau_2 = 0$, $\tau_1 > 0$. In this case, the characteristic equation at the positive equilibrium E^* takes the form

$$\lambda^2 + B_1(\tau_1)\lambda + B_2(\tau_1) + (B_3(\tau_1)\lambda + B_4(\tau_1))\, e^{-\lambda\tau_1} = 0, \tag{3.17}$$

where

$$\begin{aligned} B_1(\tau_1) &= d_2 + 2ax^* + cy^* > 0, \\ B_2(\tau_1) &= bc^2 x^* y^* > 0, \\ B_3(\tau_1) &= -(d_2 + ax^* + cy^*) < 0, \\ B_4(\tau_1) &= \frac{bcy^* k r_0 e^{-d_1\tau_1} x^*}{(1+ky^*)^2} > 0. \end{aligned}$$

Suppose $\lambda = i\omega$ (with $\omega > 0$) is a root of equation (3.17). Then $\omega(\tau_1)$ must satisfy the following

$$\begin{aligned} \omega^2 - B_2(\tau_1) &= B_3(\tau_1)\omega\sin(\omega\tau_1) + B_4(\tau_1)\cos(\omega\tau_1), \\ B_1(\tau_1)\omega &= B_4(\tau_1)\sin(\omega\tau_1) - B_3(\tau_1)\omega\cos(\omega\tau_1). \end{aligned} \tag{3.18}$$

This leads to the following equation

$$\omega^4 + D_1(\tau_1)\omega^2 + D_2(\tau_1) = 0, \tag{3.19}$$

where

$$\begin{aligned} D_1(\tau_1) &= B_1^2(\tau_1) - 2B_2(\tau_1) - B_3^2(\tau_1), \\ D_2(\tau_1) &= B_2^2(\tau_1) - B_4^2(\tau_1). \end{aligned}$$

Since $\tau_2 = 0$, then $x^* = \frac{m_2}{bc}$, and in this case y^* depends only on τ_1, condition (3.4) reduces to

$$r_0 e^{-d_1\tau_1} > d_2 + ax^*,$$

and thus, we obtain

$$\tau_1 < \frac{1}{d_1}\ln\left(\frac{bcr_0}{d_2 bc + m_2 a}\right) =: \tau_1^*. \tag{3.20}$$

We consider only the case where $D_2(\tau_1) < 0$. Then, for all $\tau_1 \in [0, \tau_1^*)$, equation (3.19) has a unique positive root

$$\omega_2 = \sqrt{\frac{-D_1(\tau_1) + \sqrt{\Delta_2}}{2}}, \quad \text{where } \Delta_2 = D_1^2(\tau_1) - 4D_2(\tau_1).$$

From equation (3.18), we obtain

$$\begin{aligned} \sin\omega\tau_1 &= \frac{B_3(\tau_1)\omega(\omega^2 - B_2(\tau_1)) + B_1(\tau_1)B_4(\tau_1)\omega}{B_4^2(\tau_1) + B_3^2(\tau_1)\omega^2} =: Q_2(\tau_1), \\ \cos\omega\tau_1 &= \frac{B_4^2(\tau_1)(\omega^2 - B_2(\tau_1)) - B_1(\tau_1)B_3(\tau_1)\omega^2}{B_4^2(\tau_1) + B_3^2(\tau_1)\omega^2} =: P_2(\tau_1). \end{aligned} \tag{3.21}$$

$I_2 = \{\tau_1 : \tau_1 \in [0, \tau_1^*),\ D_2(\tau_1) < 0\}$. For $\tau_1 \in I_2$, let $\eta(\tau_1) \in [0, 2\pi]$ be the solution to $\sin\eta(\tau_1) = Q_2(\tau_1)$, $\cos\eta(\tau_1) = P_2(\tau_1)$. Then we have

$$\omega_2(\tau_1)\tau_1 = \eta(\tau_1) + 2j\pi, \quad j = 0, 1, 2, \ldots.$$

Denote

$$R_j(\tau_1) := \tau_1 - \frac{\eta(\tau_1) + 2j\pi}{\omega_2(\tau_1)} = 0,\ j = 0, 1, 2, \ldots.$$

It follows that $\lambda = \pm i\omega_2$ with $\omega_2 > 0$ are a pair of purely imaginary roots of equation (3.17) if and only if τ_1 is a root of $R_j(\tau_1)$ for some j.

Suppose the critical value is $\tau_1 = \hat{\tau}_1$, and $\lambda(\hat{\tau}_1) = \pm i\omega_2(\hat{\tau}_1)$. Then,

$$\delta_2(\hat{\tau}_1) := \operatorname{sign}\left\{ \frac{d\,\mathrm{Re}\,\lambda}{d\tau_1}\bigg|_{\lambda = i\,\omega_2(\hat{\tau}_1)} \right\} = \operatorname{sign}\left\{ \frac{dR_j(\tau_1)}{d\tau_1}\bigg|_{\tau_1=\hat{\tau}_1} \right\}.$$

If $\delta_2(\hat{\tau}_1) \neq 0$, the transversality condition holds, and a Hopf bifurcation occurs at $\tau_1 = \hat{\tau}_1$.

Our theoretical analysis shows that the maturation delays of prey and predator populations, denoted by τ_1 and τ_2, influence not only the existence of the equilibria but also their local and global stability. In the absence of both delays (i.e., $\tau_1 = \tau_2 = 0$), the positive equilibrium is always globally asymptotically stable. However, introducing a single maturation delay-either for the prey or the predator-may lead to stability switches as the delay increases. Numerical simulations in the next section show that for Cases 2 and 3, the positive equilibrium may exhibit a stability-instability-stability transition. In contrast, when both maturation delays are considered simultaneously, the characteristic equation contains multiple delay terms (including a mixed-delay term), which is given in Case 4 below.

Case 4: $\tau_1 > 0$, $\tau_2 > 0$. When we consider both maturation delays, the characteristic equation at E^* takes the form

$$\begin{aligned} &\lambda^2 + P_1(\tau_1,\tau_2)\lambda + P_2(\tau_1,\tau_2) + P_3(\lambda,\tau_1,\tau_2)e^{-\lambda\tau_1} \\ &\quad + \left[P_4(\tau_1,\tau_2) + P_5(\lambda,\tau_1,\tau_2)\right]e^{-\lambda\tau_2} + P_6(\tau_1,\tau_2)e^{-\lambda(\tau_1+\tau_2)} = 0, \end{aligned} \tag{3.22}$$

where

$$\begin{aligned} P_1(\tau_1,\tau_2) &= m_2 + d_2 + 2ax^* + cy^*, \\ P_2(\tau_1,\tau_2) &= m_2(d_2 + 2ax^* + cy^*), \\ P_3(\lambda,\tau_1,\tau_2) &= -(d_2 + ax^* + cy^*)(\lambda + m_2), \\ P_4(\tau_1,\tau_2) &= bc^2x^*y^*e^{-m_1\tau_2}, \\ P_5(\lambda,\tau_1,\tau_2) &= -m_2(\lambda + d_2 + 2ax^* + cy^*), \\ P_6(\tau_1,\tau_2) &= m_2(d_2 + ax^* + cy^*) + bcy^*e^{-m_1\tau_2}\frac{kr_0x^*e^{-d_1\tau_1}}{(1+ky^*)^2}. \end{aligned}$$

Note that (3.22) is a very complicated transcendental equation. Time delays appear not only through the exponential factors $e^{-\lambda\tau_1}$ and $e^{-\lambda\tau_2}$, but also via the mixed term $e^{-\lambda(\tau_1+\tau_2)}$. Moreover, the equilibrium (x^*, y^*) itself depends on τ_1 and τ_2 through terms such as $e^{-d_1\tau_1}$ and $e^{-m_1\tau_2}$, so the expressions $P_i\,(i = 1, 2, \ldots, 6)$ are delay-dependent. When one searches for purely imaginary root $\lambda = i\omega$ of (3.22), then the equation for ω still has τ_1 and τ_2 in its coefficients. Thus, one cannot compute exactly the values of τ_1 and τ_2 at which stability switches occur. In addition, the feasibility of the positive equilibrium requires $x^* > 0$ and $y^* > 0$, while (x^*, y^*) varies with the delays, these constraints must be taken into account. For these reasons, we rely on numerical tools (bifurcation diagrams, delay-embedding phase portraits, and sensitivity-to-initial-data tests) to characterize stability changes and complex dynamics induced by the coupled delays.

4 Numerical simulations

Given the structural complexity of (3.22) under the coupled dual delays, it is difficult to derive unified analytical critical conditions. Therefore, in this section, we will use MATLAB-based

numerical simulations to validate the results in Section 3 and to further reveal bifurcations and complex oscillatory behaviors under both single-delay and dual-delay settings. The parameters of model (2.3) are specified as follows

$$\tau_1 = 0,\ r_0 = 2,\ k = 15,\ d_2 = 0.01,\ a = 0.01,\ c = 0.08,\ b = 0.4,\ m_1 = 0.1,\ m_2 = 0.1. \tag{4.1}$$

Using the parameter set in (4.1), we obtain $\tau_2^* = 41.5387$.

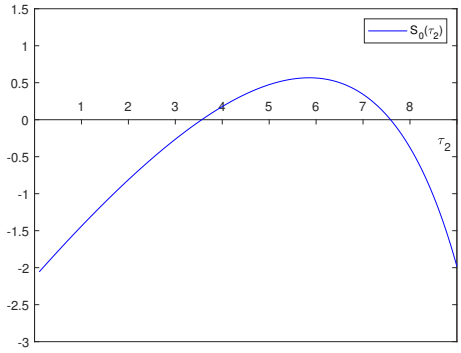

Figure 4.1: Bifurcation diagram for model (2.3) when $\tau_1 = 0$.

Figure 4.1 illustrates how the function $S_0(\tau_2)$ varies with the predator maturation delay τ_2 over the interval I_1. As shown in Figure 4.1, the graph of $S_0(\tau_2)$ has two zeros located at $\tau_{21} = 3.56$ and $\tau_{22} = 7.58$. $S_n(\tau_2)$ does not have positive roots for any $n \geq 1$. A stability switch from stable to unstable occurs at τ_{21}, followed by a transition back to stability at τ_{22}. This implies that intermediate delays $\tau_2 \in (3.56, 7.58)$ have a destabilizing effect on the steady state, whereas smaller delays $0 \leq \tau_2 < \tau_{21}$ and larger delays $\tau_2 > 7.58$ exert a stabilizing influence. Therefore, the steady state is unstable for $\tau_2 \in (\tau_{21}, \tau_{22})$, and asymptotically stable for $0 \leq \tau_2 < \tau_{21}$ and $\tau_2 > \tau_{22}$. Figure 4.2 numerically confirms the predicted stability transitions shown in Figure 4.1 through time series simulations.

Figure 4.3 considers the case when there is no juvenile predator mortality (i.e., $m_1 = 0$), and plots the curves of $S_0(\tau_2)$, $S_1(\tau_2)$ and $S_2(\tau_2)$. The intersection points of these functions with the τ_2-axis represent the critical delay values at which the characteristic equation of the positive equilibrium has a pair of purely imaginary roots. Figure 4.1 and Figure 4.3 reveal several key differences. When $m_1 = 0$, the positive equilibrium E^* remains feasible (i.e., biologically meaningful) for all $\tau_2 \geq 0$. Whereas when $m_1 > 0$, E^* only exists within a finite range of τ_2, and the system undergoes stability switches (see Figure 4.1). However, when $m_1 = 0$ (see Figure 4.3), once τ_2 exceeds the first critical value, E^* loses stability permanently. In addition, as τ_2 increases further, the curves $S_1(\tau_2)$ and $S_2(\tau_2)$ successively cross zeros, suggesting the onset of increasingly complex dynamics beyond simple periodic oscillations. These predictions are validated by the numerical simulations shown in Figure 4.4, where large values of τ_2 lead to the emergence of highly irregular oscillatory behaviors. This striking difference in dynamics highlights the critical role of juvenile predator mortality (m_1) in shaping the long-term impact of time delays in stage-structured population models. A similar phenomenon was also investigated in [11].

Figure 4.5 shows the bifurcation diagram of the predator population density with respect to time delay τ_2, using the same parameter set as in Figure 4.1. For small τ_2, the curve represents the stable equilibrium density of predators. As τ_2 crosses the first Hopf bifurcation

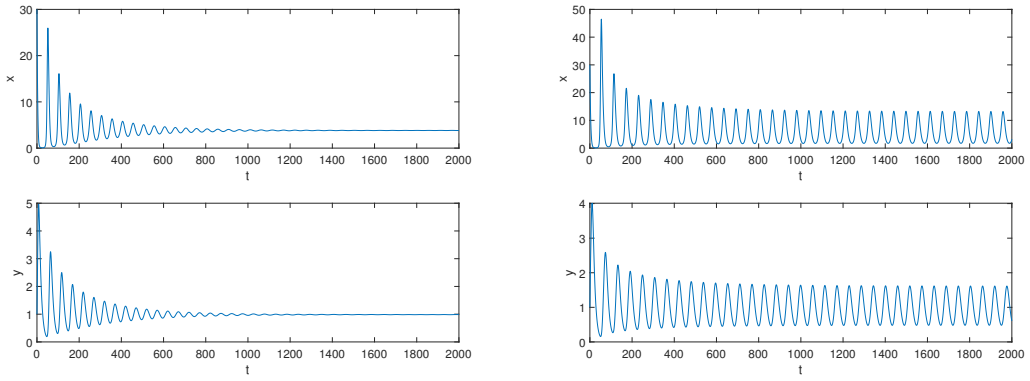

(a) $\tau_2 = 2$ (b) $\tau_2 = 5$

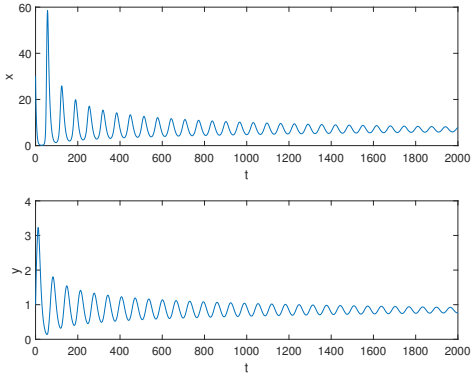

(c) $\tau_2 = 8$

Figure 4.2: Time series diagrams of model (2.3) for different values of time delay τ_2 with $\tau_1 = 0$.

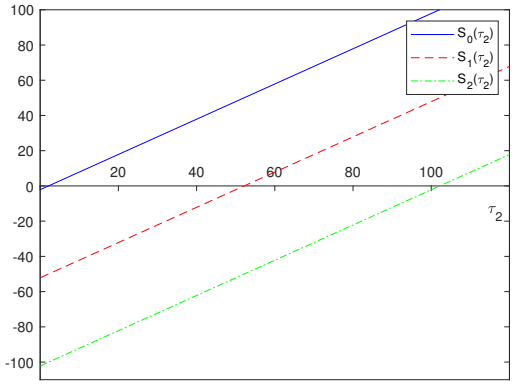

Figure 4.3: Plots of the functions $S_0(\tau_2)$, $S_1(\tau_2)$, $S_2(\tau_2)$ when $m_1 = 0$.

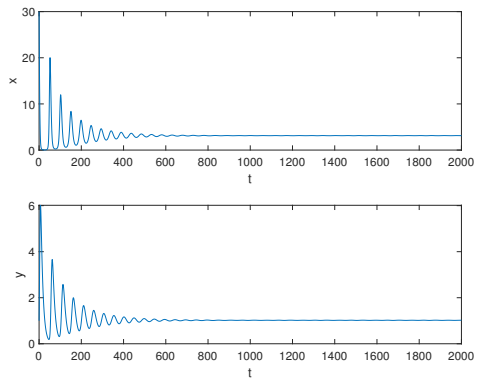

(a) $\tau_2 = 1$

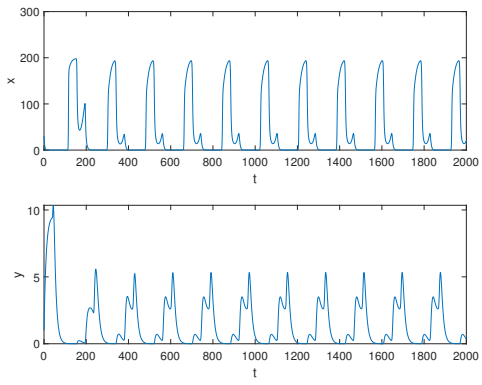

(b) $\tau_2 = 40$

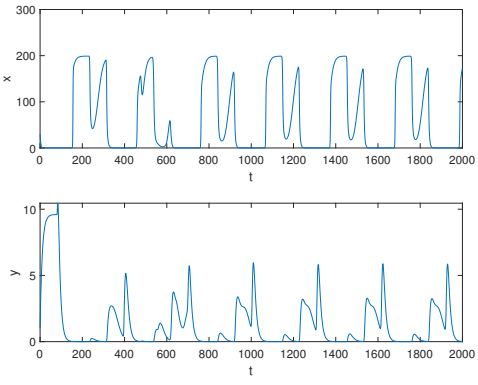

(c) $\tau_2 = 80$

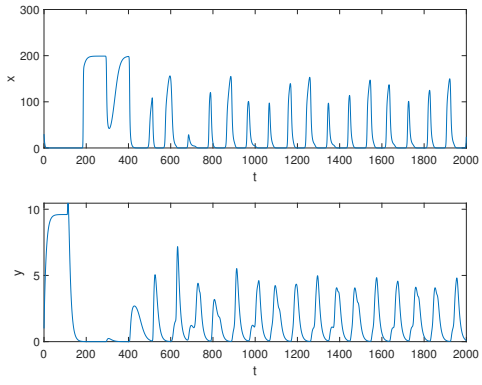

(d) $\tau_2 = 110$

Figure 4.4: Time series diagrams of model (2.3) as τ_2 varies and $\tau_1 = 0$, $m_1 = 0$.

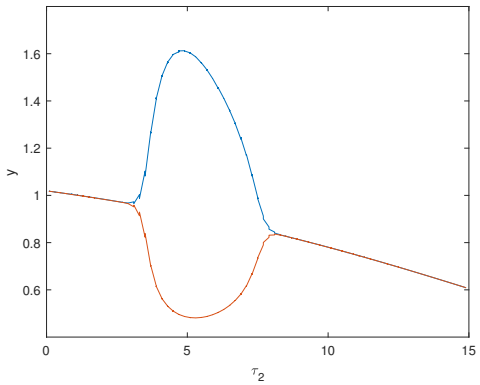

Figure 4.5: Bifurcation diagram of predators with respect to parameter τ_2 with $\tau_1 = 0$.

point, the curve bifurcates into two branches, a stable limit cycle appears. The time series shown in Figure 4.2 are consistent with the bifurcation structure illustrated in Figure 4.5.

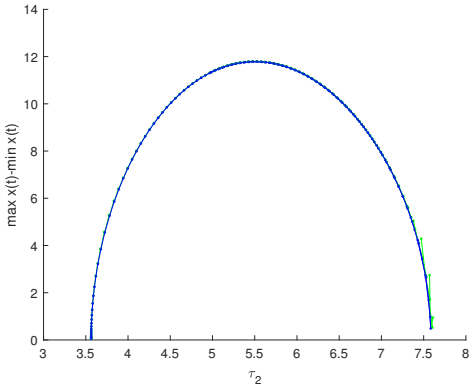

Figure 4.6: Global Hopf branches of model (2.3) when $\tau_1 = 0$.

The global Hopf bifurcation branches were computed using the MATLAB package DDE-BIFTOOL [7, 8], and the results are presented in Figure 4.6. Figure 4.6 illustrates the global Hopf bifurcation structure of the system under the condition $\tau_1 = 0$ and $\tau_2 > 0$. As τ_2 increases, the system undergoes a Hopf bifurcation, transitioning from a stable equilibrium to periodic oscillatory behavior. Further increase in τ_2 eventually suppresses the oscillations, leading the system back to a stable state, the limit cycle disappears and the positive equilibrium regains its stability.

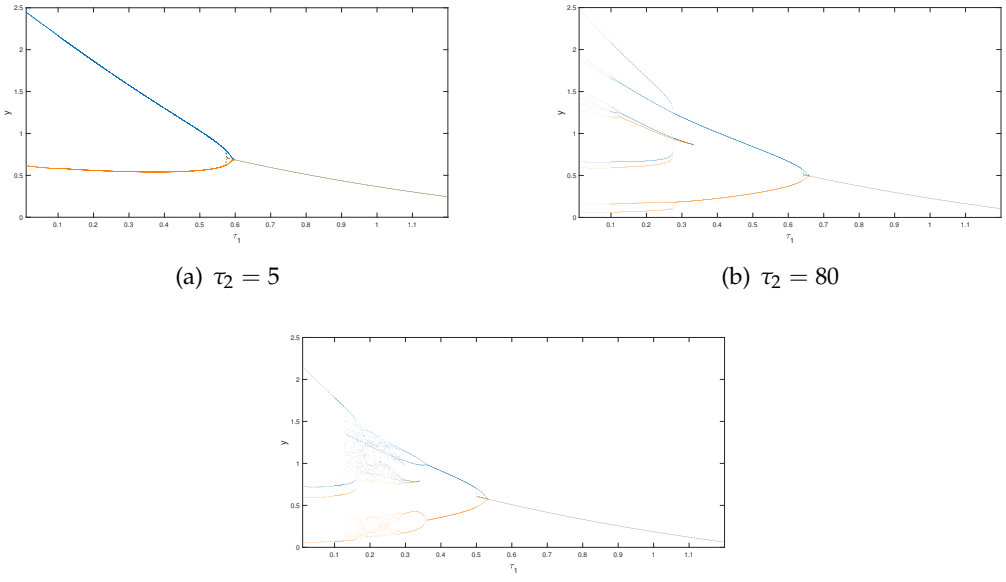

(a) $\tau_2 = 5$ (b) $\tau_2 = 80$

(c) $\tau_2 = 92$

Figure 4.7: Bifurcation diagram showing local maxima (blue) and minima (orange) of $y(t)$ as τ_1 varies for different values of $\tau_2 = 5, 80, 92$.

For completeness, we also examined the complementary setting by fixing $\tau_2 = 0$ and treating τ_1 as the bifurcation parameter. The resulting bifurcation patterns, stability switches,

and oscillatory behaviors are qualitatively similar to those obtained for $\tau_1 = 0$ with varying τ_2; to avoid repetition, the corresponding figures are omitted.

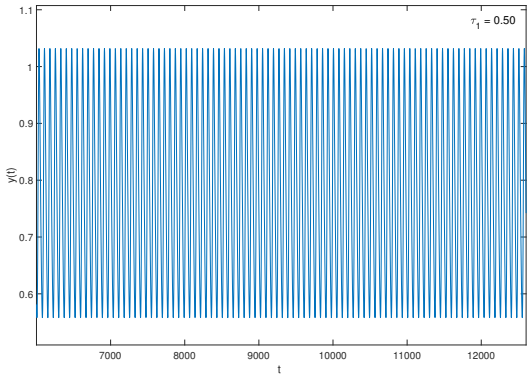

(a) $\tau_1 = 0.5$, $\tau_2 = 5$

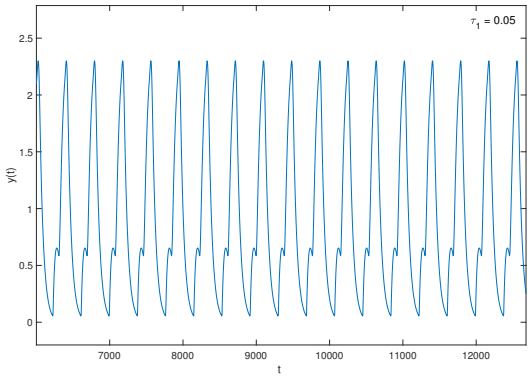

(b) $\tau_1 = 0.05$, $\tau_2 = 80$

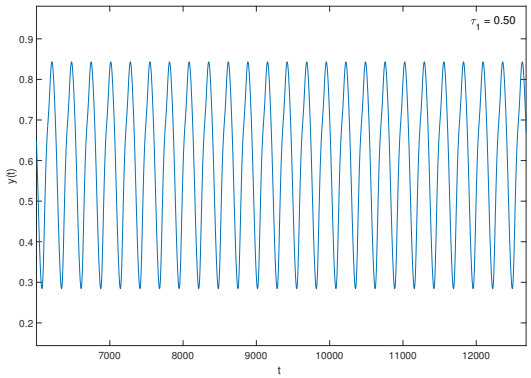

(c) $\tau_1 = 0.5$, $\tau_2 = 80$

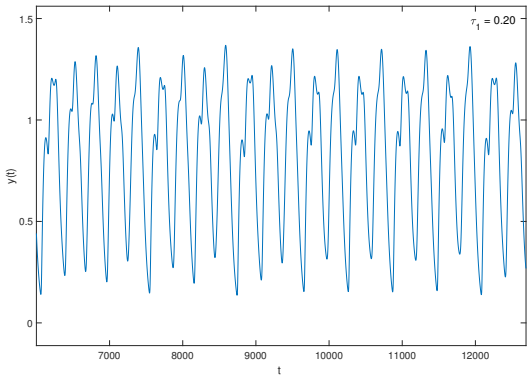

(d) $\tau_1 = 0.2$, $\tau_2 = 92$

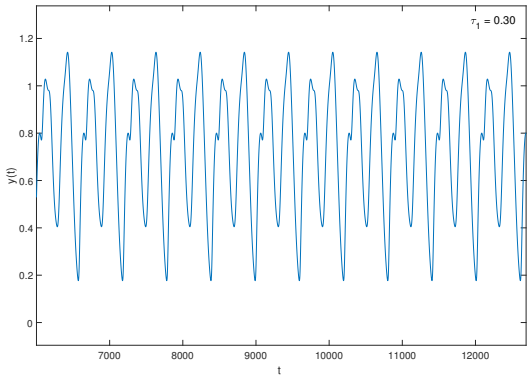

(e) $\tau_1 = 0.3$, $\tau_2 = 92$

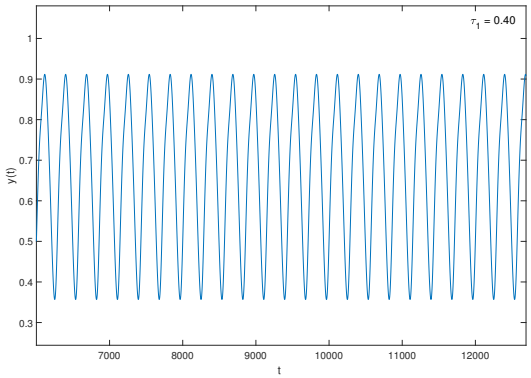

(f) $\tau_1 = 0.4$, $\tau_2 = 92$

Figure 4.8: Time series diagrams of model (2.3) for different values of time delay τ_1 and τ_2.

In Figures 4.1–4.6, we mainly illustrate the delay-induced stability changes and oscillation-

generation mechanisms of model (2.3) under simplified delay settings by fixing one of the two delays at zero. It should be emphasized that model (2.3) involves two discrete delays, τ_1 and τ_2, whose coupled effects may significantly alter the bifurcation structure and the types of long-term attractors. To systematically characterize the dynamical behaviors when both delays coexist, unless otherwise stated, we fix the remaining parameters as

$$r_0 = 2, \quad d_1 = 1, \quad d_2 = 0.28, \quad a = 1, \quad c = 1, \quad b = 0.34, \quad m_1 = 0.016, \quad m_2 = 0.02, \quad k = 0.1$$

and then vary the values of τ_1 and τ_2. By combining time series, delay-embedding phase portraits, and sensitivity tests with respect to initial histories, we reveal complex dynamical mechanisms induced by the coupled dual delays.

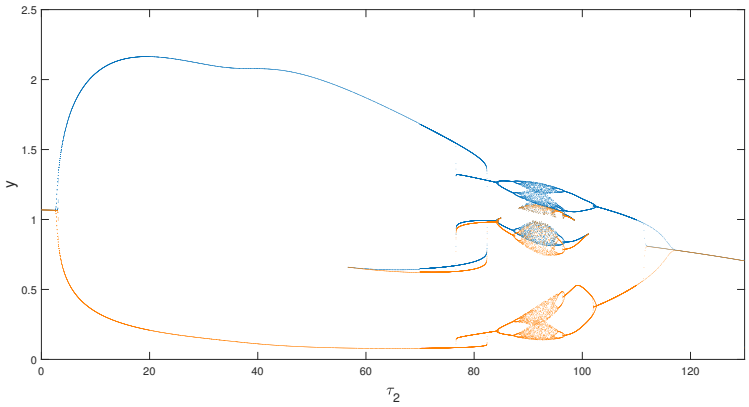

Figure 4.9: Bifurcation diagram of predators with respect to parameter τ_2 with $\tau_1 = 0.25$.

In Figure 4.7, we fix three different values of τ_2 (namely, $\tau_2 = 5, 80, 92$), and plot the local maxima (blue) and local minima (orange) of $y(t)$ as τ_1 varies to form an extrema-based bifurcation diagram. When $\tau_2 = 5$, the branches are almost two smooth single-valued curves, indicating that as τ_1 varies the system mainly exhibits a stable equilibrium or a regular single-period oscillation, and the dynamics remain relatively simple. When $\tau_2 = 80$, branch splitting and discontinuities appear over part of the τ_1 range (approximately $\tau_1 \in [0, 0.28]$), suggesting a pronounced increase in branching complexity that may be associated with multibranch long-term behaviors (e.g., coexisting attractors). When τ_2 is further increased to 92, a dense cloud of extrema emerges for τ_1 in the range of approximately $[0.11, 0.27]$, indicating more complex irregular oscillations that may correspond to chaos or strongly aperiodic attractors. Overall, as τ_2 increases, for each fixed τ_2, the increase in time delay τ_1 exhibits a substantial rise in dynamical complexity, with the branch structure evolving from regular single-valued branches to multibranch patterns and even to a scattered cloud. This demonstrates that τ_2 plays a key role in modulating the system's response to τ_1: the two delays are not independent, but jointly shape stability and bifurcation behaviors through their coupling.

To further elucidate the dynamical behaviors associated with the different branch structures in Figure 4.7, we select several representative parameter points and plot the corresponding time series, as shown in Figure 4.8. When $\tau_2 = 5$ and $\tau_1 = 0.5$ (Figure 4.8(a)), the time series exhibits a regular single-period oscillation. Figures 4.8(b) and 4.8(c) correspond to two representative points in Figure 4.7 with $\tau_2 = 80$, namely $\tau_1 = 0.05$ (the small-τ_1 branch band) and $\tau_1 = 0.5$, respectively. Although these two points lie on different extrema levels in the

bifurcation diagram (reflecting different amplitudes), both time series display stable periodic oscillations, indicating that periodic attractors still dominate the dynamics at these parameter values. Meanwhile, the nearly parallel branches and branch discontinuities observed in the small-τ_1 region of Figure 4.7 suggest a possible multibranch structure in that interval (e.g., potential attractor coexistence). When $\tau_2 = 92$ and $\tau_1 = 0.2$ (Figure 4.8(d)), the waveform is no longer strictly repetitive; both the amplitude and the spacing between peaks and troughs fluctuate markedly, showing complex irregular oscillations consistent with the thickened cloud of extrema in the corresponding interval of Figure 4.7. For $\tau_1 = 0.3$ (Figure 4.8(e)) and $\tau_1 = 0.4$ (Figure 4.8(f)), the system exhibits period-doubled oscillations and single-period oscillations, respectively, indicating that as τ_1 increases the dynamics can re-enter periodic windows from the complex irregular regime. Overall, Figures 4.7 and 4.8 corroborate each other: for smaller τ_2 the dynamics are mainly regular periodic oscillations, whereas for larger τ_2, as τ_1 increases, the system can produce richer and more diverse dynamical behaviors.

To further characterize the organizing role of τ_2 in shaping the dynamical structure, Figure 4.9 presents an extrema-based bifurcation diagram of model (2.3) obtained by fixing $\tau_1 = 0.25$ and scanning τ_2, where the local maxima (blue) and local minima (orange) of $y(t)$ are plotted. The numerical results show that the system transitions from a stable equilibrium to an oscillatory branch near $\tau_2 \approx 2.5$, and returns from oscillations to a stable equilibrium near $\tau_2 \approx 116.7$. In addition, around $\tau_2 \approx 76.5$ and $\tau_2 \approx 82.7$, branch splitting and discontinuous segments are observed, suggesting the possible presence of multiple attractors. Furthermore, period-doubling and periodic windows can be detected for certain ranges of τ_2 (e.g., representative period-doubled orbits at $\tau_2 = 83, 87, 87.5, 88.4, 95.5, 95.7, 97, 105$), while a relatively wide scattered band appears for $\tau_2 \approx$ 90-95, indicating that the system may enter a chaotic regime or a strongly quasi-periodic state. Overall, varying τ_2 drives alternating transitions between regular periodic motion and complex irregular dynamics. Figures 4.7 (τ_2 is fixed, τ_1 varies) and 4.9 (τ_1 is fixed, τ_2 varies) together reveal the bifurcation structure and complex dynamical regions induced by the coupled dual delays.

To validate the typical dynamical behaviors associated with different τ_2-intervals in Figure 4.9, Figure 4.10 plots representative time series of $y(t)$ (left) together with the corresponding delay-embedding portraits $(y(t-\tau_2),\, y(t))$ (right) for selected values of τ_2. Figures 4.10(a)-(d) show that when τ_2 increases through $\tau_2 = 83$, 87, 87.5, and 88.4, the time series remains periodic, while the delay-embedding portraits exhibit approximately 1, 2, 4, and 8 closed loops, respectively, forming a hierarchical pattern consistent with 2^n growth ($n = 0, 1, 2, 3$). This is consistent with a period-doubling cascade, where periodic solutions evolve from T to $2T$, $4T$, and $8T$.

Figure 4.11 shows that when $\tau_2 = 93$, the time series is no longer strictly repetitive and the embedded trajectory becomes thickened and intricately intertwined, suggesting chaotic or strongly aperiodic dynamics.

To further illustrate the reappearance of periodic windows after the scattered region in Figure 4.9, Figure 4.12(a)–(d) display the time series and delay-embedding portraits for $\tau_2 =$ 95.5, 95.7, 97, and 105. The results show that the system returns to relatively regular periodic oscillations at these values, with closed orbits in the embedding plane; moreover, the numbers of closed loops are approximately 8, 4, 2, and 1, respectively, exhibiting a 2^n-type decreasing hierarchy. This suggests that after the scattered (complex) segment, the dynamics gradually return from higher-order multi-period orbits to lower-order periodic orbits. These observations further highlight the key role of the delay parameter τ_2 in organizing the bifurcation structure and the periodicity of the system. It is worth noting that such delay-induced

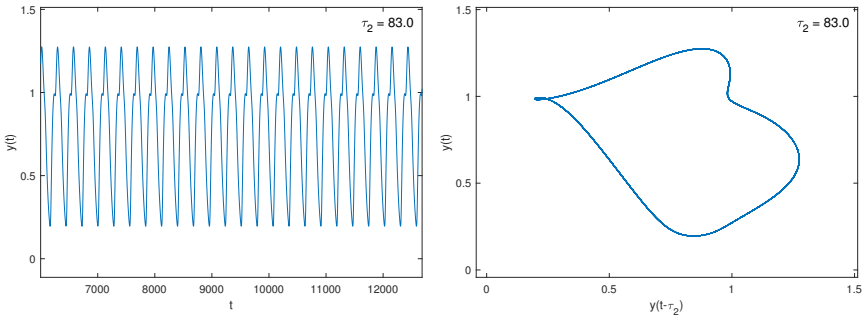

(a)

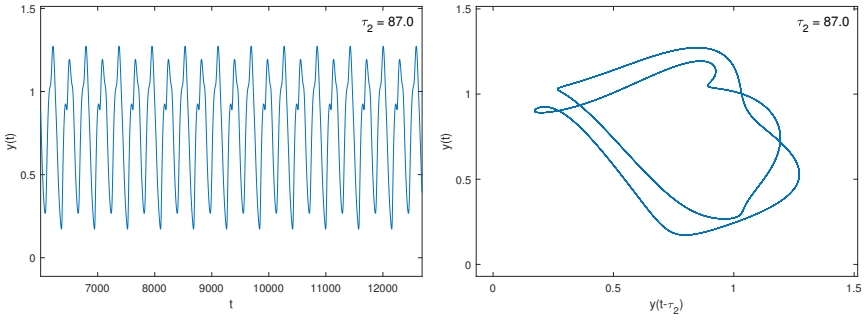

(b)

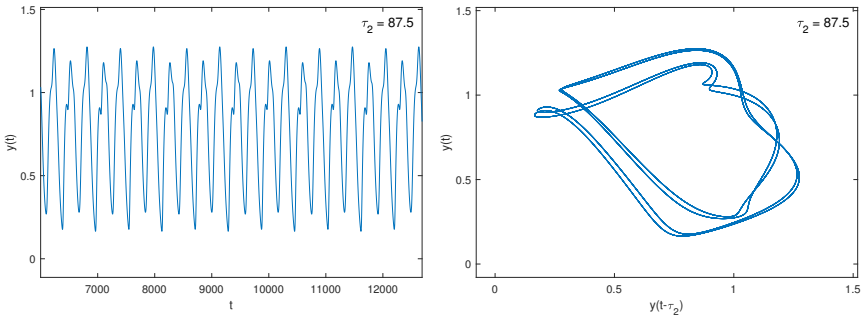

(c)

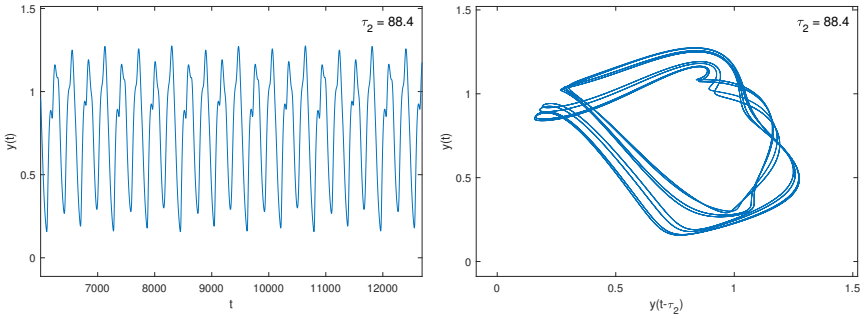

(d)

Figure 4.10: Solution curves of model (2.3) with $\tau_1 = 0.25$ and different values of τ_2 ($\tau_2 = 83, 87, 87.5, 88.4$).

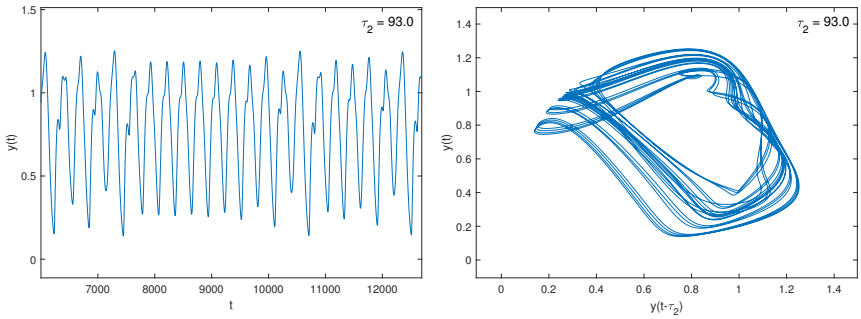

Figure 4.11: Solution curves of model (2.3) with $\tau_1 = 0.25$ and $\tau_2 = 93$.

period-doubling cascades, periodic windows, and complex irregular oscillations are qualitatively similar to the dynamical patterns reported by Fan and Wolkowicz [9] for a discrete-delay predator–prey model.

To test the sensitivity of the complex segment in the bifurcation diagram (Figure 4.9) to initial history functions, Figure 4.13 compares simulations starting from two constant history functions on $t \in [-\tau, 0]$: the solid curve corresponds to $x(t) = y(t) = 0.1$, whereas the dashed curve corresponds to $x(t) = 0.11$ and $y(t) = 0.1$, i.e., only a small perturbation is applied to x. The left panel shows the tail time series for $\tau_2 = 93$, where the two trajectories separate clearly over time, indicating strong sensitivity to the initial history and suggesting that the dynamics at this parameter value are characterized by complex, aperiodic behavior typical of chaotic systems. The right panel shows the tail time series for $\tau_2 = 97$, where the two curves almost overlap without persistent divergence, implying that the attractor is closer to a stable periodic orbit. Overall, Figure 4.13 demonstrates that the system responds weakly to small perturbations in periodic regimes, whereas in the complex (aperiodic) regime small perturbations can be significantly amplified.

In Figure 4.14, we fix $\tau_2 = 81.5$ and construct the delay-embedding portrait $(y(t-\tau_2), y(t))$ for two different constant history initializations on $t \in [-\tau, 0]$: the blue dashed curve corresponds to $x(t) = 0.1$, $y(t) = 0.1$, and the red solid curve corresponds to $x(t) = 0.2$, $y(t) = 0.8$. After the numerical solutions enter their long-term stable evolution, the trajectories do not converge to the same orbit; instead, they form two distinguishable closed curves in the embedding plane. The blue dashed orbit covers a larger region with higher oscillation amplitude, while the red solid orbit is more contracted with smaller amplitude. Estimating the dominant period from inter-peak intervals after transients decay yields approximately 335.62 for the blue dashed periodic attractor and approximately 277.96 for the red solid periodic attractor. Therefore, for the same parameter value $\tau_2 = 81.5$, the system admits two stable periodic attractors, exhibiting a typical attractor coexistence (bistability) phenomenon. This also provides a plausible mechanism for the branch splitting and discontinuous structures observed in Figures 4.7 and 4.9.

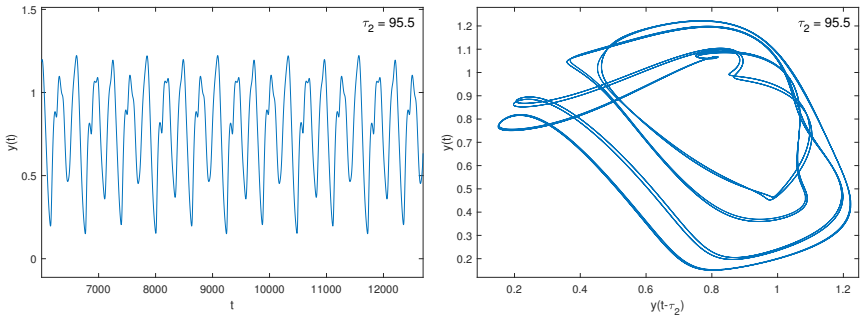

(a)

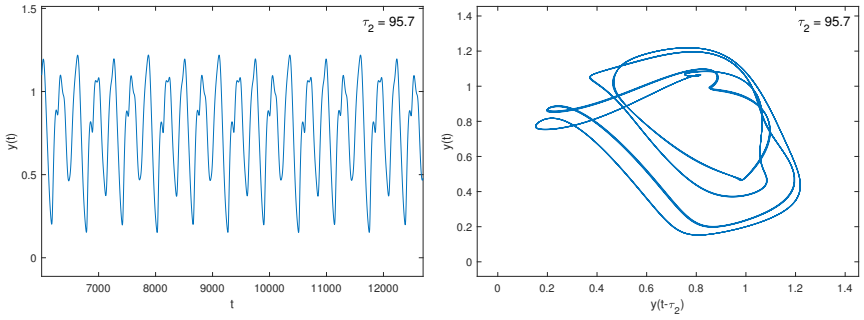

(b)

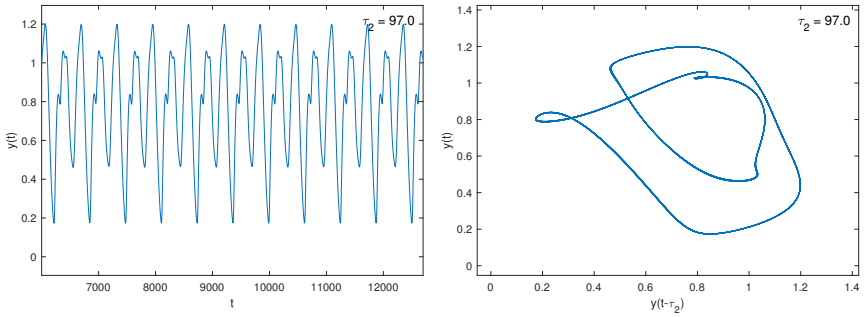

(c)

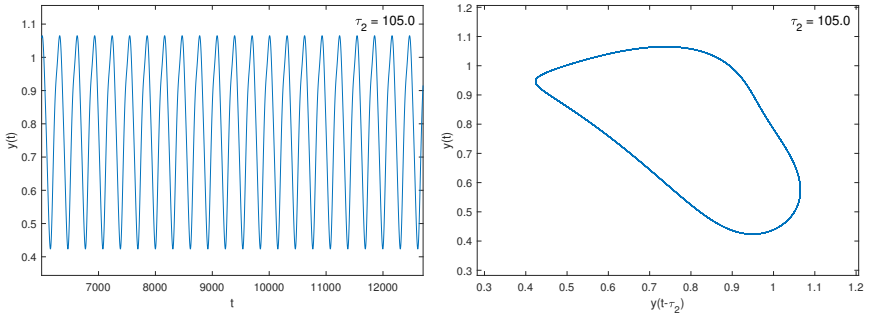

(d)

Figure 4.12: Solution curves of model (2.3) with $\tau_1 = 0.25$ and different values of τ_2 ($\tau_2 = 95.5, 95.7, 97, 105$).

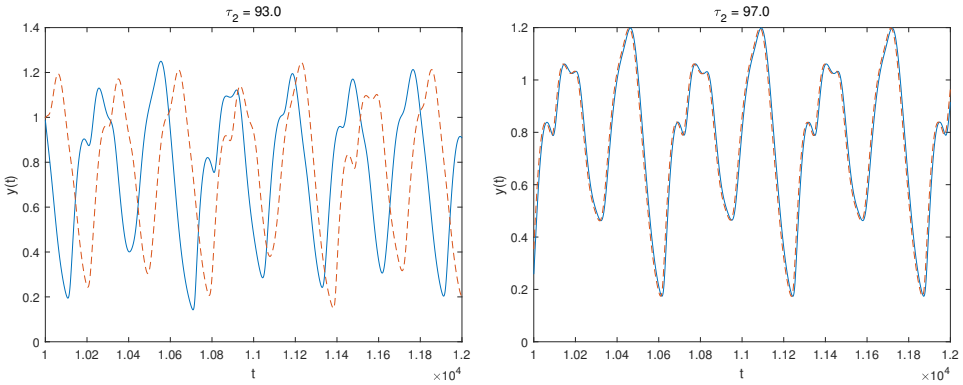

Figure 4.13: Time series at $\tau_2 = 93$ and $\tau_2 = 97$ for histories $x(t) = y(t) = 0.1$ (blue solid) and $x(t) = 0.11$, $y(t) = 0.1$ (red dashed), illustrating strong and weak sensitivity to a small perturbation.

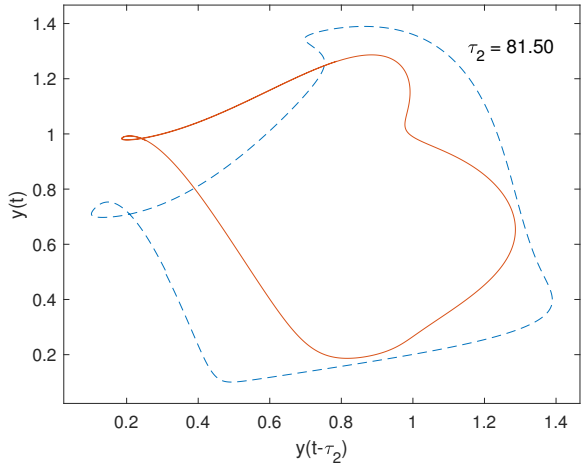

Figure 4.14: Time-delay embedding $\big(y(t-\tau_2), y(t)\big)$ at $\tau_2 = 81.5$ showing two coexisting stable periodic attractors: blue dashed $(x(t) = 0.1, y(t) = 0.1)$ and red solid $(x(t) = 0.2, y(t) = 0.8)$.

5 Conclusions and discussions

We formulate a delayed predator–prey model that incorporates both dual-stage structure and two distinct maturation delays. A comprehensive dynamical analysis is conducted to investigate the effects of these ecological mechanisms on the behavior of system. Theoretical results demonstrate that all solutions of modle (2.3) remain non-negative and ultimately bounded. By the corresponding characteristic equations and comparison principle, we establish both local and global stability criteria for the equilibria in model (2.3), and identify conditions under which Hopf bifurcations may occur. Specifically, when the effective reproductive rate of juvenile prey satisfies $r_0 e^{-d_1\tau_1} \leq d_2$, the extinction equilibrium E_0 is globally asymptotically stable (see Theorem 3.1). This result implies that a sufficiently low juvenile survival rate inevitably leads to population extinction. If $r_0 e^{-d_1\tau_1} > d_2$, but the predator's conversion efficiency is too low (i.e., $m_2 > bP(x_1)e^{-m_1\tau_2}$), then the predator-free equilibrium E_1 becomes globally stable (see Theorem 3.2, emphasizing the critical importance of energy transfer efficiency for predator–prey coexistence. In contrast, when the predator conversion efficiency exceeds this threshold (i.e., $m_2 < bP(x_1)e^{-m_1\tau_2}$), a positive interior equilibrium arises, indicating the potential for stable long-term coexistence between prey and predator populations.

Numerical simulations are conducted to support and extend the theoretical results. In the single-delay setting (fix one delay at zero), increasing the delay parameter causes the system dynamics to shift from stability to oscillation, and then return to stability. Bifurcation diagrams and time-series analyses confirm that these transitions are caused by Hopf bifurcations. Moreover, neglecting juvenile mortality leads to more complex system dynamics as time delays increase. This highlights the critical importance of juvenile survival for maintaining ecological stability. When both delays are present, through the extrema-based bifurcation scans with respect to τ_1 and τ_2, a richer organization of branching structures can be observed, including multibranch patterns, local jumps and discontinuities, and scattered clouds of extrema in certain parameter intervals, suggesting transitions between regular periodic oscillations and more complex irregular dynamics. The delay-embedding portraits further reveal typical structures such as period-doubling cascades and the return of periodic windows. On the one hand, within the scattered-cloud and complex regimes, sensitivity tests to initial histories show that the system is highly history-dependent: small perturbations in the initial history may lead to pronounced long-term trajectory separation, supporting the interpretation that these regimes may correspond to complex attractors (e.g., strongly aperiodic dynamics). On the other hand, in parameter ranges where branch splitting and discontinuities are more pronounced, numerical comparisons under different history initializations indicate attractor coexistence: for the same parameter value, multiple stable periodic attractors may coexist. This provides a mechanistic explanation for the multibranch structures observed in the bifurcation diagrams. Therefore, compared with the Hopf-type stability switching typically observed in single maturation-delay models (e.g., [11, 21]), the coupled two-maturation-delay case can further exhibit richer dynamical structures, including branch splitting, period-doubling windows, reappearance of periodic windows, and stronger sensitivity to the initial data.

From the perspective of stage structure and time delays, our analysis reveals that population renewal efficiency–represented by terms like $e^{-d_1\tau_1}$ and $e^{-m_1\tau_2}$-plays a key role in shaping the system's stability landscape. These results offer important theoretical insights into the complex dynamic interactions and feedback mechanisms within ecological systems. In the current model, only adult predators are assumed to have predatory capability and are restricted to feeding on adult prey. This assumption is supported by observations in certain

bird-insect systems, where juvenile birds primarily rely on food provided by parents or feed on abundant, non-limiting resources, whereas adult birds typically prey on larger, fully developed insects. However, this simplification may not hold universally. Future extensions of the model could incorporate juvenile predatory behavior. Moreover, population migration is common in the world and plays an important role in the population dynamics. We leave this as our future work.

Acknowledgements

This research was supported by the Natural Science Basic Research Plan in Shaanxi Province of China (2024JC-YBMS-001, 2025JC-YBMS-004).

References

[1] W. G. Aiello, H. I. Freedman, J. Wu, Analysis of a model representing stage-structured population growth with state-dependent time delay, *SIAM J. Appl. Math.* **52**(1992), No. 3, 855–869. https://doi.org/10.1137/0152048; MR1163810; Zbl 0760.92018

[2] Q. An, E. Beretta, Y. Kuang, C. Wang, H. Wang, Geometric stability switch criteria in delay differential equations with two delays and delay dependent parameters, *J. Differential Equations* **266**(2019), No. 11, 7073–7100. https://doi.org/10.1016/j.jde.2018.11.025; MR3926093; Zbl 1414.34056

[3] R. Banerjee, P. Das, D. Mukherjee, Effects of fear and anti-predator response in a discrete system with delay, *Discrete Contin. Dyn. Syst. Ser. B.* **27**(2022), No. 7, 3643–3661. https://doi.org/10.3934/dcdsb.2021200; MR4430632; Zbl 1501.92104

[4] E. Beretta, Y. Kuang, Geometric stability switch criteria in delay differential systems with delay dependent parameters, *SIAM J. Math. Anal.* **33**(2002), No. 5, 1144–1165. https://doi.org/10.1137/S0036141000376086; MR1897706; Zbl 1013.92034

[5] S. Chen, J. Shi, J. Wei, Time delay-induced instabilities and Hopf bifurcations in general reaction-diffusion systems, *J. Nonlinear Sci.* **23**(2013), No. 1, 1–38. https://doi.org/10.1007/s00332-012-9138-1; MR3023084; Zbl 1271.34071

[6] B. Dai, G. Sun, Turing–Hopf bifurcation of a delayed diffusive predator–prey system with chemotaxis and fear effect, *Appl. Math. Lett.* **111**(2021), 106644. https://doi.org/10.1016/j.aml.2020.106644; MR4128587; Zbl 1450.35045

[7] K. Engelborghs, T. Luzyanina, G. Samaey, DDE-BIFTOOL v. 2.00: A MATLAB package for bifurcation analysis of delay differential equations, Department of Computer Science, K.U. Leuven, Leuven, Belgium, Tech. Rep. TW-330, 2001.

[8] K. Engelborghs, T. Luzyanina, D. Roose, Numerical bifurcation analysis of delay differential equations using DDE-BIFTOOL, *ACM Trans. Math. Software* **28**(2002), No. 1, 1–21. https://doi.org/10.1145/513001.513002; MR1918642; Zbl 1070.65556

[9] G. Fan, G. S. K. Wolkowicz, Chaotic dynamics in a simple predator–prey model with discrete delay, *Discrete Contin. Dyn. Syst. Ser. B* **26**(2021), No. 1, 191–216. https://doi.org/10.3934/dcdsb.2020263; MR4191543; Zbl 1468.34111

[10] S. A. Gourley, Y. Kuang, Wavefronts and global stability in a time-delayed population model with stage structure, *Proc. R. Soc. Lond. Ser. A Math. Phys. Eng. Sci.* **459**(2003), No. 2034, 1563–1579. https://doi.org/10.1098/rspa.2002.1094; MR1994271; Zbl 1047.92037

[11] S. A. Gourley, Y. Kuang, A stage structured predator–prey model and its dependence on maturation delay and death rate, *J. Math. Biol.* **49**(2004), No. 2, 188–200. https://doi.org/10.1007/s00285-004-0278-2; MR2145690; Zbl 1055.92043

[12] S. Halder, J. Bhattacharyya, S. Pal, Comparative studies on a predator–prey model subjected to fear and Allee effect with type I and type II foraging, *J. Appl. Math. Comput.* **62**(2020), No. 1, 93–118. https://doi.org/10.1007/s12190-019-01275-w; MR4056893; Zbl 1478.92155

[13] J. K. Hale, S. M. Verduyn Lunel, *Introduction to functional differential equations*, Appl. Math. Sci., Vol. 99, Springer-Verlag, New York, 1993. https://doi.org/10.1007/978-1-4612-4342-7; Zbl 0787.34002

[14] Y. Kuang, *Delay differential equations with applications in population dynamics*, Math. Sci. Eng., Vol. 191, Academic Press, Boston, MA, 1993. MR1218880; Zbl 0777.34002

[15] L. Lai, X. Yu, M. He, Z. Li, Impact of Michaelis–Menten type harvesting in a Lotka–Volterra predator–prey system incorporating fear effect, *Adv. Differential Equations* **2020**(2020), Papar No. 320, 22 pp. https://doi.org/10.1186/s13662-020-02724-8; MR4118442; Zbl 1485.92094

[16] J. Li, Y. Kuang, Analysis of a model of the glucose-insulin regulatory system with two delays, *SIAM J. Appl. Math.* **67**(2007), No. 3, 757–776. https://doi.org/10.1137/050634001; MR2300309; Zbl 1115.92015

[17] T. Li, Q. Wang, Turing patterns in a predator–prey reaction-diffusion model with seasonality and fear effect, *J. Nonlinear Sci.* **33**(2023), No. 5, 86. https://doi.org/10.1007/s00332-023-09938-6; MR4621539; Zbl 1520.35167

[18] Z. Liang, X. Meng, Stability and Hopf bifurcation of a delayed predator–prey model with a stage structure for generalist predators and a Holling type-II functional response, *Symmetry* **16**(2024), No. 5, 597. https://doi.org/10.3390/sym16050597

[19] S. Liu, L. Chen, G. Luo, Y. Jiang, Asymptotic behaviors of competitive Lotka–Volterra system with stage structure, *J. Math. Anal. Appl.* **271**(2002), No. 1, 124–138. https://doi.org/10.1016/S0022-247X(02)00103-8; MR1923751; Zbl 1022.34039

[20] J. Liu, Y. Kang, Spatiotemporal dynamics of a diffusive predator–prey model with fear effect, *Nonlinear Anal. Model. Control* **27**(2022), No. 5, 841–862. https://doi.org/10.15388/namc.2022.27.27465; MR4477173; Zbl 1498.92169

[21] X. Ma, Y. Su, X. Zou, Joint impact of maturation delay and fear effect on the population dynamics of a predator–prey system, *SIAM J. Appl. Math.* **84**(2024), No. 4, 1557–1579. https://doi.org/10.1137/23M1596569; MR4775676; Zbl 1555.34095

[22] P. Panday, S. Samanta, N. Pal, J. Chattopadhyay, Delay induced multiple stability switch and chaos in a predator–prey model with fear effect, *Math. Comput. Simulation* **172**(2020), 134–158. https://doi.org/10.1016/j.matcom.2019.12.015; MR4066199; Zbl 1510.92177

[23] H. Qi, X. Meng, Threshold behavior of a stochastic predator–prey system with prey refuge and fear effect, *Appl. Math. Lett.* **113**(2021), 106846. https://doi.org/10.1016/j.aml.2020.106846; MR4168272; Zbl 1459.92091

[24] D. Sahoo, G. P. Samanta, Impact of fear effect in a two prey-one predator system with switching behaviour in predation, *Differ. Equ. Dyn. Syst.* **32**(2024), No. 2, 377–399. https://doi.org/10.1007/s12591-021-00575-7; MR4721735; Zbl 1533.92177

[25] S. Samaddar, M. Dhar, P. Bhattacharya, Effect of fear on prey–predator dynamics: Exploring the role of prey refuge and additional food, *Chaos* **30**(2020), No. 6, 063129. https://doi.org/10.1063/5.0006968; MR4109555; Zbl 1440.92058

[26] H. Shu, W. Xu, X. S. Wang, J. Wu, Complex dynamics in a delay differential equation with two delays in tick growth with diapause, *J. Differential Equations* **269**(2020), No. 12, 10937–10963. https://doi.org/10.1016/j.jde.2020.07.029; MR4150363; Zbl 1511.34086

[27] X. Wang, L. Zanette, X. Zou, Modelling the fear effect in predator–prey interactions, *J. Math. Biol.* **73**(2016), No. 5, 1179–1204. https://doi.org/10.1007/s00285-016-0989-1; MR3555366; Zbl 1358.34058

[28] X. Wang, X. Zou, Modeling the fear effect in predator–prey interactions with adaptive avoidance of predators, *Bull. Math. Biol.* **79**(2017), No. 6, 1325–1359. https://doi.org/10.1007/s11538-017-0287-0; MR3662108; Zbl 1372.92095

[29] Y. Wang, X. Zou, On a predator–prey system with digestion delay and anti-predation strategy, *J. Nonlinear Sci.* **30**(2020), No. 4, 1579–1605. https://doi.org/10.1007/s00332-020-09618-9; MR4113337; Zbl 1445.34121